Revista Mexicana de Física **43**, *No. 4 (1997) 533–544*

Frequency multiplexed quasi-distributed fiber-optic interferometric sensor

M.G. SHLYAGIN, S.V. MIRIDONOV, AND D. TENTORI
Centro de Investigación Científica y de Educación de Ensenada
Apartado postal 2732, 22880 Ensenada, B.C., Mexico

Recibido el 7 de febrero de 1997; aceptado el 2 de abril de 1997

ABSTRACT. The operation of a new quasi-distributed interferometric sensor is discussed. The sensor is based on an array of unbalanced interferometers formed by point polarization couplers along a birefringent fiber. The simultaneous interrogation of the sensing interferometers was achieved by using spectroscopic methods and a simple signal processing. Experimental verification of sensor operation and the analysis of cross-talk and system noise is presented.

RESUMEN. Se discute el funcionamiento de un nuevo tipo de sensor cuasi-distribuido. El sensor está basado en un arreglo de interferómetros desbalanceados, formados por acopladores puntuales de polarización, localizados a lo largo de una fibra birrefringente. La interrogación simultánea de los interferómetros sensores se llevó a cabo utilizando métodos espectroscópicos y un procesado de señales sencillo. Se presenta tanto la verificación experimental del funcionamiento del sensor, como el análisis del cruzamiento de señales y de el ruido del sistema.

PACS: 42.81.Pa; 42.81.Cn; 42.81.Qb

1. INTRODUCTION

Interferometric optical sensors with spectral encoding of information attracted considerable research interest because of their high potential sensitivity and ability to provide absolute measurements. There are two basic approaches to encode sensed information. The first one makes use of the resonant spectral response of periodical structures like in-fiber Bragg grating (FBG). An external influence changes resonance conditions and causes a shift of the output spectral line. In these sensors demodulation is achieved by measuring the wavelength shift of the resonant spectral line from a calibrated position. Shift of the resonant wavelength of FBG is typically so small that it leads to the problem of interrogation and demultiplexing of output signals from a series of FBG elements, in particular, when measuring static and quasi-static fields [1].

The second approach is based on the modulation of the intensity spectrum of a broad band light source by two beam either Mach-Zender or Michelson interferometers, or by the Fabry-Perot interferometer. Here, the modulation function serves as an output signal and its frequency is proportional to the optical path imbalance of the interferometer and, therefore, is sensitive to any external influence that changes optical parameters of the interferometer. This approach was demonstrated in different experimental configurations,

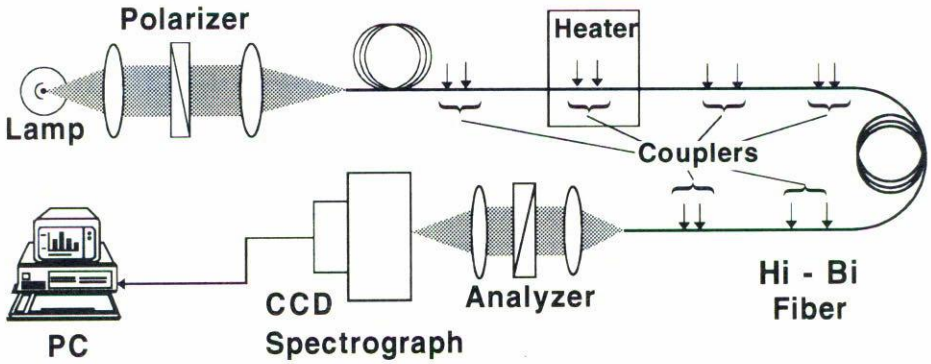

FIGURE 1. Schematic diagram of the quasi-distributed sensor.

mainly for single point sensors [3–5]. Quasi-distributed fiber-optic sensing using this principle is very attractive but problematic because of the complexity of construction and networking of interferometric sensors.

A possible way to overcome this problem is the use of interferometric sensors formed by point-like polarization couplers within a single-length polarization-maintaining fiber. Our preliminary experiments have shown the high potential of this approach for quasi-distributed fiber-optic sensing [6]. We formed a serial array of in-fiber unbalanced interferometers by using point-like polarization couplers placed along a polarization-maintaining fiber. Portions of the fiber between adjacent coupling points work as unbalanced interferometers. Optical path imbalances of sensing interferometers depend on temperature and strain and can be measured with a broad band light source. Simultaneous interrogation of the sensing interferometers was achieved by using spectroscopic methods and a simple signal processing.

Here we present the results of investigation of this new quasi-distributed sensor capable of measuring the isotropic fields, such as temperature, through the change induced on the intrinsic birefringence of a polarization maintaining fiber.

2. PRINCIPLE OF OPERATION

A schematic diagram of the interferometric quasi-distributed sensor is shown in Fig. 1. The sensor consists of a polarization-maintaining fiber with a number of point-like polarization mode couplers distributed along the fiber length. The couplers are grouped in pairs with different distances between couplers in different pairs. We refer below as local sensors the sections of the fiber having one pair of couplers. Operation of the sensor is based on dependence of a fiber birefringence on external influences such as temperature, strain, etc. By monitoring changes of birefringence in each local sensor it is possible to detect variations of temperature and strain at different locations simultaneously.

To detect these variations, white light is launched into one principal mode of the fiber and the output spectrum of the second mode is measured. While propagating along the fiber, part of the optical power from the first principal mode is transfered into the second mode at those points where couplers are located. So, each local sensor consisting of

two point couplers produces two new light wave components in the second mode. There is some distance between couplers in a local sensor, and, due to birefringence of the fiber, there is a phase difference between these two components which depends on the wavelength. Hence the interference of these two new components results in sinusoidal modulation of the output spectrum of the second mode. If the distances between couplers in different local sensors are not equal to each other then the frequencies of this periodical modulation in the output spectrum will be unique for each local sensor and therefore separate detection of birefringence variations at different locations becomes possible. Below we consider the theory of operation of such a sensor and analyze possible limitations of its performance.

2.1. THEORY

We use Jones formalism to describe the operation of this local sensor representing a light wave propagating along the fiber as a vector consisting of complex amplitudes of each orthogonal mode and the point couplers and fiber segments as matrices. Using this approach, the light at the output end of the fiber can be written as

$$\begin{pmatrix} a_{\text{out1}} \\ a_{\text{out2}} \end{pmatrix} = \mathbf{P}_N \, \mathbf{K}_{N-1} \, \mathbf{P}_{N-1} \ldots \mathbf{K}_1 \, \mathbf{P}_1 \, \mathbf{K}_0 \mathbf{P}_0 \begin{pmatrix} a_{\text{in1}} \\ a_{\text{in2}} \end{pmatrix}, \tag{1}$$

where a_{in1}, a_{in2}, a_{out1}, and a_{out2} are the complex amplitudes of the eigenmodes at the input and output ends of the fiber, $\mathbf{K}$ and $\mathbf{P}$ are coupling and propagation matrices:

$$\mathbf{K}_l = \begin{pmatrix} 1 - |y_l|^2/2 & iy_l \\ iy_l^* & 1 - |y_l|^2/2 \end{pmatrix} \quad \text{and} \quad \mathbf{P}_l = \begin{pmatrix} e^{i\delta(z_l - z_{l-1})/2} & 0 \\ 0 & e^{-\delta(z_l - z_{l-1})/2} \end{pmatrix}. \tag{2}$$

Here z_l are the coordinates along the fiber where point couplers are located ($z_N = L$, and $z_{-1} = 0$; where L is the total fiber length), δ is the propagation constant difference for two modes:

$$\delta = \frac{2\pi \Delta n}{\lambda}, \tag{3}$$

where Δn is the intrinsic birefringence of the fiber, λ is light wavelength, and y_l is the coupling coefficient which reflects the strength of mode transfer at l-th coupler. To simplify the analysis, we assume that $|y_l| \ll 1$ and, more strictly, the total coupling is so small that the condition

$$\sum_{l=0}^{N-1} |y_l|^2 \ll 1 \tag{4}$$

is satisfied. In other words, we use here a linear approximation to describe the operation of the fiber optic sensor under consideration.

As was mentioned above, to detect the variations of birefringence caused by temperature or strain, white light is launched into one principal mode of the fiber and the output spectrum of the other mode is measured. Let us suppose that mode a_2 with amplitude 1 is launched into the fiber. Using condition (4) we can simplify (1) as

$$a_{\text{out1}} \approx \sum_{l=0}^{N-1} i\, y_l e^{i\delta(L-2z_l)/2} \qquad \text{and} \qquad a_{\text{out2}} \approx e^{-iL\delta/2}, \tag{5}$$

and represent measured output light intensity of mode a_1 as

$$|a_{\text{out1}}|^2 \approx \left| \sum_{l=0}^{N-1} i y_l e^{i\delta(L-2z_l)/2} \right|^2 = \sum_{l,m=0}^{N-1} y_l\, y_m^*\, e^{i\delta(z_m - z_l)}. \tag{6}$$

One can see that due to spectral dependence of parameter δ (Eq. 3), the output spectrum (6) is a superposition of sine waves along the wavenumber scale ($\nu = 1/\lambda$). Theoretically all these sinusoidal components can be detected separately using a Fourier transform of the output spectrum. However, not all these components are necessary to retrieve the information about the birefringence variations in different local sensors. If there are M coupler pairs in the sensor, then (6) can be converted into

$$\begin{aligned} |a_{\text{out1}}|^2 \approx & \sum_{l=0}^{M-1} \left(|y_{2l}|^2 + |y_{2l+1}|^2\right) + \sum_{l=0}^{M-1} \left[y_{2l}\, y_{2l+1}^*\, e^{i\delta(z_{2l} - z_{2l+1})} + y_{2l}^*\, y_{2l+1}\, e^{-i\delta(z_{2l} - z_{2l+1})} \right] \\ & + \sum_{l=0}^{M-2} \left[y_{2l+1}\, y_{2l+2}^*\, e^{i\delta(z_{2l+1} - z_{2l+2})} + y_{2l+1}^*\, y_{2l+2}\, e^{-i\delta(z_{2l+1} - z_{2l+2})} \right] \\ & + \sum_{l=0}^{2M-1} \sum_{|m-l|>1}^{2M-1} y_l\, y_m^*\, e^{i\delta(z_m - z_l)}. \end{aligned} \tag{7}$$

The first term in this expression gives a constant component which has no spectral dependence. The second term represents the sum of sine signals whose frequencies on the wavenumber scale are proportional to the distance between point couplers of individual pairs. Other terms correspond to the sum of sine signals with frequencies related to the distances between couplers that belong to different pairs. As was mentioned above, the distance between pairs was chosen much greater than the distance between point couplers within individual pairs, hence the sine signal frequencies in the third and fourth terms are much higher than those in the second term. If the shortest distance between different pairs exceeds L_{min}:

$$L_{\text{min}} = \frac{1}{\Delta n\, \Delta\nu}, \tag{8}$$

where $\Delta\nu$ is the spectral resolution of the spectrograph along the wavenumber scale, the spectrograph itself acts as a low-pass filter and rejects sine signals with high frequencies. Using this assumption, and taking into account that $\delta = 2\pi\Delta n\nu$, the output spectrum can be written as

$$|a_{\text{out1}}|^2 \approx \sum_{l=0}^{M-1} \left(|y_{2l}|^2 + |y_{2l+1}|^2\right) + 2 \sum_{l=0}^{M-1} |y_{2l}\, y_{2l+1}| \cos\left(2\pi\Delta n\, \Delta z_l\, \nu + \Delta\phi_l\right), \tag{9}$$

where Δz_l is the distance between couplers in l-th local sensor, $\Delta\phi_l = \arg(y_{2l}) - \arg(y_{2l+1})$.

Distance between couplers in each individual pair were different from each other, and, therefore, each pair of couplers (local sensor) produced its own cosine signal in the output spectrum with frequency $f_l = \Delta n\, \Delta z_l$. Since distances between couplers in all pairs are known, this allows us to distinguish the signals from different local sensors even if the information about their position is not explicitly present in the output spectrum (9).

The frequencies $f_l = \Delta n\, \Delta z_l$ in (9) related to different local sensors also depend on the value of the intrinsic birefringence Δn of the fiber between the couplers in individual pairs, so if the distances within all pairs are known, fiber birefringence and its changes may be evaluated. For example, one pair of point couplers was used to measure the birefringence dispersion in Ref. 8. This can also be useful for sensors of isotropic fields. Fields, such as temperature do not lead to intermode coupling, hence they can not be measured through the evaluation of coupling coefficients y_l. However, a change of the isotropic field may induce a change on the local birefringence $\delta(\Delta n)$ of the fiber between couplers of the correspondent local sensor. This change can be detected as a shift of frequency of the cosine signal related to this pair

$$\delta f_l = \delta(\Delta n)\, \Delta z_l, \tag{10}$$

hence the evaluation of the position of the correspondent peak gravity center within the Fourier transformed output spectrum enables to estimate the change of the external field surrounding the l-th local sensor.

Since the intrinsic birefringence Δn also depends on the wavelength, the compensation of this dispersion may be necessary. This can be done through a nonlinear transformation of the wavenumber scale performed introducing a modified wavenumber $\nu_{\mathrm{mod}} = \nu\Delta n(\nu)/\Delta n(\nu_c)$. The procedure used to represent the discrete output signal along a modified wavenumber scale is described in Ref. 7.

2.2. Linear approximation and cross-talk noise

As was mentioned above, the principle of operation of the fiber-optic sensor here presented has been described using a linear approximation which significantly simplifies the analysis. It was assumed that coupling coefficients at coupling points are very small. However, one can see that small coupling coefficients lead, in turn, to a poor power transfer from the launched mode into the other one. This can produce very weak signals difficult to detect in the presence of photodetector noise and/or optical noise caused by fiber imperfections and uncontrollable mechanical forces. On the other hand, if the coupling is strong enough to produce a powerful signal at the output of the optical fiber, another problem may arise. Multiple power conversion from one mode to another may result in the appearance of cross-talk noise: nonlinear components in the output spectrum. Therefore, the analysis of both situations is required to determine the boundaries in which the sensor should operate.

Let us discuss the cross-talk problem first. In the previous section we have shown that the output spectrum after the analyzer is a superposition of sine waves along the wave number scale with frequencies $f_0, f_2, \ldots, f_{M-1}$, corresponding to M different local

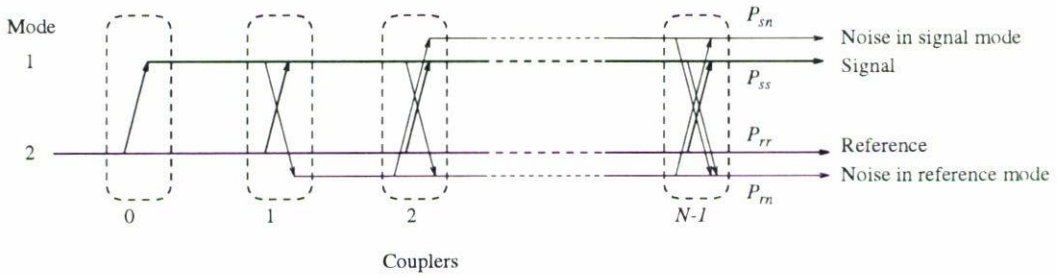

FIGURE 2. Cross talk noise in polarimetric quasi-distributed fiber-optic sensors. The power conversion occurs between reference and signal modes in both directions. Conversion from the initial reference mode rises the signal carrying information about the characteristics of local sensors. Back conversion from signal to reference mode creates new components which, in turn, being transfered into the signal mode again will produce cross-talk noise with amplitude dependent on the characteristics of several other local sensors

sensors (pairs of couplers). When the coupling coefficients do not satisfy condition (4) the output signal contains not only *true* components with these frequencies, but also *false* components with other frequencies. The mechanism of rising cross-talk noise is illustrated by Fig. 2.

The comprehensive analysis of cross-talks is rather complicated, however an acceptable accuracy of evaluation of the cross-talk level can be achieved using also a simplified model of power conversion. We will analyze the propagation of two modes through one point coupler, considering one mode a_1 as signal mode and another (a_2) as reference mode. This consideration is chosen because in our particular example [see Eq. (5)] mode a_1 carries useful information about the state of local sensors while mode a_2 plays the role of reference and pump wave to provide the power and reference phase for signal mode a_1. In our analysis, we split both modes into two components: noiseless part and noise component.

Signal mode a_1 is considered as the sum of a signal component a_{ss} with average power $P_{\mathrm{ss}} = \langle |a_{\mathrm{ss}}|^2 \rangle$ and a noise component a_{sn} with average power $P_{\mathrm{sn}} = \langle |a_{\mathrm{sn}}|^2 \rangle$. The complex amplitude of the signal component a_{ss} consists only of terms which are linearly dependent on the coupling coefficients of the couplers [same as in Eq. (5)] due to single power conversion from noiseless component of the reference mode. The noise component of the signal mode a_{sn} contains all other terms: coupling coefficients of order higher than one and their products coming from multiple power conversions.

The first component of the reference mode is a pure reference component a_{rr} whose amplitude changes when part of its energy is coupled into signal. Phase will depend only on the distance from the input end of the fiber. The average power of this component is $P_{\mathrm{rr}} = \langle |a_{\mathrm{rr}}|^2 \rangle$. The complex amplitude of the second component a_{rn} of the reference mode consists of terms which appear due to back conversion of part of the signal mode into the reference mode. Because of multiple conversions, its amplitude will contain terms with coupling coefficients of order higher than one as well as their products. These terms are considered here as noise in the reference mode. The average power of this component is $P_{\mathrm{rn}} = \langle |a_{\mathrm{rn}}|^2 \rangle$.

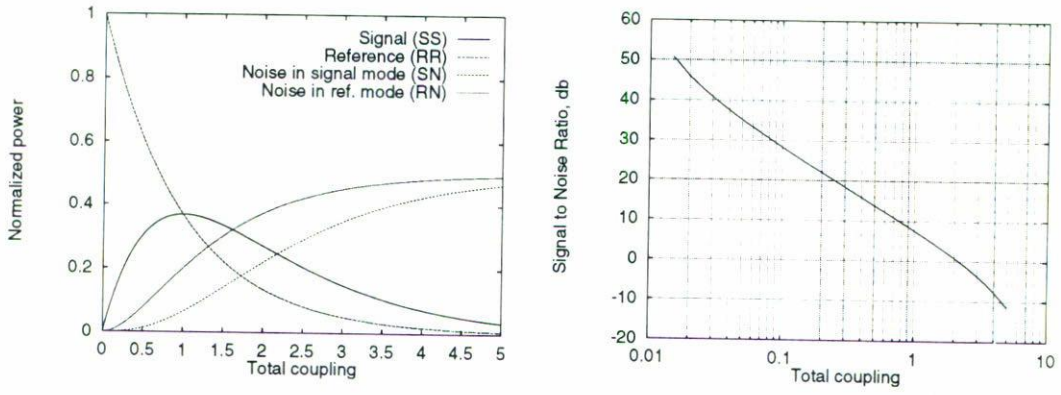

FIGURE 3. Evolution of signal, reference and cross-talk noise power (a), and signal-to-noise ratio in the signal mode (b): $P_{\rm ss}/P_{\rm sn}$. Total coupling here is the average coupling coefficient K of one coupler multiplied by the number of couplers $2M$.

We consider an arbitrary m-th coupler in the fiber sensor. Light entering through the input of this coupler may already contain signal and noise components and we will analyze, how the optical power of these components has changed after the coupler. Assuming coupling coefficients are random with average values $\langle y \rangle = 0$ and $\langle |y|^2 \rangle = K$, and statistically independent of each other ($\langle y_m\, y_n^* \rangle = 0$ for $m \neq n$), and taking into account that in our case only the reference mode is launched into the fiber (with power $P_0 = 1$), we can write recurrent expressions for the average power of each component.

At the output of the m-th coupler the power of the signal component in the signal mode is

$$P_{\rm ss}(m) = (1 - K)P_{\rm ss}(m-1) + KP_{\rm rr}(m-1). \tag{11}$$

It consists of (i) an input signal whose power is slightly reduced due to conversion into the reference mode, and (ii) a new signal term generated by power conversion from the noiseless component in the reference mode. In the reference mode, the noiseless component is slightly reduced due to power coupling into the new component of the signal (11):

$$P_{\rm rr}(m) = (1 - K)P_{\rm rr}(m-1), \tag{12}$$

All other terms in the signal and reference modes are considered as noise. The power of these noise components in the signal and reference mode is given by

$$P_{\rm sn}(m) = (1 - K)P_{\rm sn}(m-1) + KP_{\rm rn}(m-1), \tag{13}$$

and

$$P_{\rm rn}(m) = (1 - K)P_{\rm rn}(m-1) + K[P_{\rm ss}(m-1) + P_{\rm sn}(m-1)]. \tag{14}$$

The results of the computer simulation of the evolution of reference, signal and noise components in both modes are presented in Fig. 3a. Our investigation has shown that

when the coupling coefficients of point couplers are small ($K \ll 1$), the reference, signal and noise powers depend only on the total coupling $2MK$, where $2M$ is the number of point couplers along the fiber (M is a number of local sensors).

Linear regime of operation of the fiber-optic sensor can be determined using an acceptable level of cross-talk noise as a criterion. Particularly, if the required signal-to-noise ratio must be higher than 30 dB, the total coupling in the fiber has to be below 0.08. For example, if the sensor consists of 30 local sensors (60 point couplers) the coupling efficiency K of each coupler must be less than 0.13%.

It is also necessary to mention here that since the cross-talks appear due to multiple power conversion at discrete points of the fiber (where couplers are located) they will be seen as superposition of sine waves in the output spectrum along the wavenumber scale with discrete frequencies defined by the positions of the couplers. Hence proper selection of local sensors position and distances between couplers within each local sensor may help to avoid overlapping of *true* and *false* components in the Fourier transformed output spectrum and reduce the influence of cross-talk noise on the measurements results obtained from the sensor during its operation. However, this subject has yet to be investigated.

2.3. PHOTODETECTOR NOISE AND FIBER IMPERFECTIONS

Besides the cross-talk noise two other sources of noise have to be taken into account when analyzing the performance of the fiber-optic sensor here discussed. The first one is a photodetector noise and the second one is an optical noise caused by fiber imperfections.

Photodetector noise appears as random fluctuations of signal coming from the photodetector. The average signal is proportional to the mean optical power (see Eq. 9):

$$P_{\mathrm{s}} = P_0 \Big\langle \sum_{l=0}^{M-1} \left(|y_{2l}|^2 + |y_{2l+1}|^2 \right) \Big\rangle = 2MP_0 \left\langle |y|^2 \right\rangle = 2MP_0K, \tag{15}$$

where P_0 is the optical power of the launched mode at the fiber input and K is the average coupling efficiency of couplers in the local sensors. We assume that the output spectrum from the sensor is recorded by a photodetector array with N elements, and the photodetector noise in each element is characterized by its standard deviation σ_{ph}, which in units of incident optical power corresponds to the minimum detectable signal per pixel. The signal-to-noise ratio (SNR) of the photodetector system measured in decibels is

$$\mathrm{SNR}_{\mathrm{inp}} = 20 \log \left(\frac{P_{\mathrm{s}}}{\sigma_{\mathrm{ph}}} \right). \tag{16}$$

After recording, the discrete Fourier transform of the signal is calculated from N samples of the signal. The output spectrum, as it follows from (9), consists of multiple cosine signals. It is well known that if the cosine signal has an amplitude A, and there is noise with standard deviation σ_{n}, the signal-to-noise ratio in the Fourier spectrum in the sample correspondent to signal frequency is $A^2N/(2\sigma_n^2)$. In our case, in accordance with (9) $\langle A^2 \rangle = 4P_0^2 \left\langle |y_{2l}\, y_{2l+1}| \right\rangle^2 = 4P_0^2K^2$, and taking into account (15), the resultant SNR can be written as

$$\mathrm{SNR} = 10\log\left(\frac{4P_0^2K^2N}{2\sigma_{\mathrm{ph}}^2}\right) = 10\log\left(\frac{N}{2M^2}\frac{P_{\mathrm{s}}^2}{\sigma_{\mathrm{ph}}^2}\right) = \mathrm{SNR}_{\mathrm{inp}} + 10\log\left(\frac{N}{2M^2}\right). \tag{17}$$

The signal-to-noise ratio of a photodetector $\mathrm{SNR}_{\mathrm{inp}}$ may depend on many factors which are out of the frame of this work. However, we consider equation (17) to be very useful for the evaluation of the final signal-to-noise ratio in the particular implementation of a quasi-distributed sensor because value $\mathrm{SNR}_{\mathrm{inp}}$ can be easily measured or estimated. For typical photodetectors such as CCD, $N = 10^3$, and for a number of local sensors $M = 30$ the resultant signal-to-noise ratio will be 2.6 dB less than the initial SNR of the photodetector. Specific figures may vary depending on the particular application in which the sensor is used.

The optical noise caused by fiber imperfections appears as additional variations in the output spectrum due to the random transfer of optical power from the reference mode into the signal one. This power transfer is typically characterized by extinction ratio $\eta \approx hL$, where h is a polarization holding parameter and L is the total fiber length. If $hL \ll 1$, the optical power of this noise component is $P_{\mathrm{dpn}} \approx hP_0L$. This noise looks like a signal coming from many weak couplers randomly distributed along the fiber length and consists of a constant bias P_{dpn} and a variable component with standard deviation $\sigma_{\mathrm{dpn}} = P_{\mathrm{dpn}}$. In terms of frequencies of the output spectrum modulation this varying part occupies a frequency range from 0 to ΔnL. After the Fourier transform it will be spread along the entire frequency range while the signal will appear as sharp peaks. Therefore, even if the total power of this noise may be comparable with the total signal power when the length of the sensor exceeds 100–1000 meters, the contribution of this noise in a final signal-to-noise figure will be negligible. Indeed, since the spectrograph acts as a low-pass filter with cutoff frequency ΔnL_{min}; where L_{min} is defined by (8), the standard deviation of varying part of the this noise in recorded spectrum will be equal to

$$\sigma_{\mathrm{dpn}} = P_{\mathrm{dpn}}\sqrt{\frac{L_{\mathrm{min}}}{L}} = P_0h\sqrt{L_{\mathrm{min}}L}\,. \tag{18}$$

If only this noise is taken into account, the SNR after the Fourier transform is

$$\mathrm{SNR} = 10\log\left(\frac{4P_0^2K^2N}{2P_0^2h^2L_{\mathrm{min}}L}\right) = 10\log\left(\frac{2K^2N}{h^2L_{\mathrm{min}}L}\right) = 10\log\left(\frac{C_{\mathrm{total}}^2N}{2M^2h^2L_{\mathrm{min}}L}\right), \tag{19}$$

where $C_{\mathrm{total}} = 2MK$ is the total coupling. Typically $h < 10^{-5}$–10^{-4} per one meter of fiber. Our estimations show that if total coupling is 0.08, $M = 30$, $N = 10^3$ and $L = 100$ m, SNR will be in a range of 45–65 dB.

3. Experimental results

The experimental setup is shown in Fig. 1. We used a 20 W tungsten lamp as light source. Output spectra in the wavelength range from 600 to 900 nm were recorded with a 1024 element CCD detector. Wavelength resolution of the spectrograph was approximately

0.7 nm. The length of the bow-tie polarization-maintaining fiber was 80 meters. The fiber cut-off wavelength is below 600 nm and its polarization beat length is 1 mm at 650 nm. We used six pairs of coupling points with different distances between the points in different pairs. The polarization mode coupling was produced by squeezing the fiber between twists of miniature springs. In each coupling point the pressed area length was close to half of the polarization beat length at the central wavelength of the spectrum. Therefore, dependence of coupling efficiency on wavelength was very small and we could consider such coupler as point couplers. The total light intensity transfered by couplers into the output mode was less than 5% of the input mode intensity, hence the coupling coefficients were small. Neither cross-talk nor noise from fiber imperfections have been detected. As was shown, when the polarization analyzer is oriented at 90° with respect to the polarization of the launched mode, the output spectrum consists only of components, whose frequencies of oscillation are proportional to the distances between the coupling points in correspondent local sensors. In order to interrogate and demultiplex the output signals, each local sensor had a specified frequency range related with the temperature range to be measured. The local sensors were placed at random positions along the fiber, with a length of 80 m, separated by distances $d > L_{\min}$; where $L_{\min}$ is given by relation (8). For our experimental setup $L_{\min}$ was approximately equal to 1 m.

In the experiment we heated a section of the fiber where the second local sensor was placed, while the others were at an ambient temperature, as is shown in Fig. 1. The distance between the coupling points of the second local sensor was of 12 cm. To measure an axial strain we fixed the fiber on two linear translation stages with a local sensor placed between them. Strain was applied by a controlled displacement of one stage.

Signal processing included the following steps: an output spectrum recording, representation of the spectrum with a modified wavenumber ν_{mod} using data on dispersion measurements from Ref. 8, and the fast Fourier transform. We determined precisely the frequency of the signal for each local sensor by using the modules of the Fourier transform, and by calculating the frequency position of the gravity center of the corresponding peak. The Fourier transform of a signal is shown in Fig. 4a. Six peaks at different frequencies clearly indicate the signals from the six local sensors. When the temperature of a local sensor changes, the position of the corresponding peak in the Fourier spectrum also changes. Thus, the difference between the measured frequency and that one obtained with the calibration procedure at a known temperature gives us the absolute temperature for each sensor. Experimental results of the calibration of the sensor are shown in Figs. 4b and 4c. The small amplitude periodic oscillation of the temperature measured for the first local sensor is the result of the interference with the side lobes of the signal coming from the second local sensor. These two sensors have a minimum frequency separation. Data in Fig. 4b for the fifth local sensor illustrate that such errors become significantly smaller in the case of a large frequency separation.

The sensitivity of the sensor is determined by precision of signal frequency measurement which, in turn, depends on a noise level. To estimate threshold sensitivity we measured the frequencies of the signals several times with constant temperature and axial strain. Standard deviation of random errors was of the order of 0.05°C for temperature measurement and 20 μstrain for axial strain.

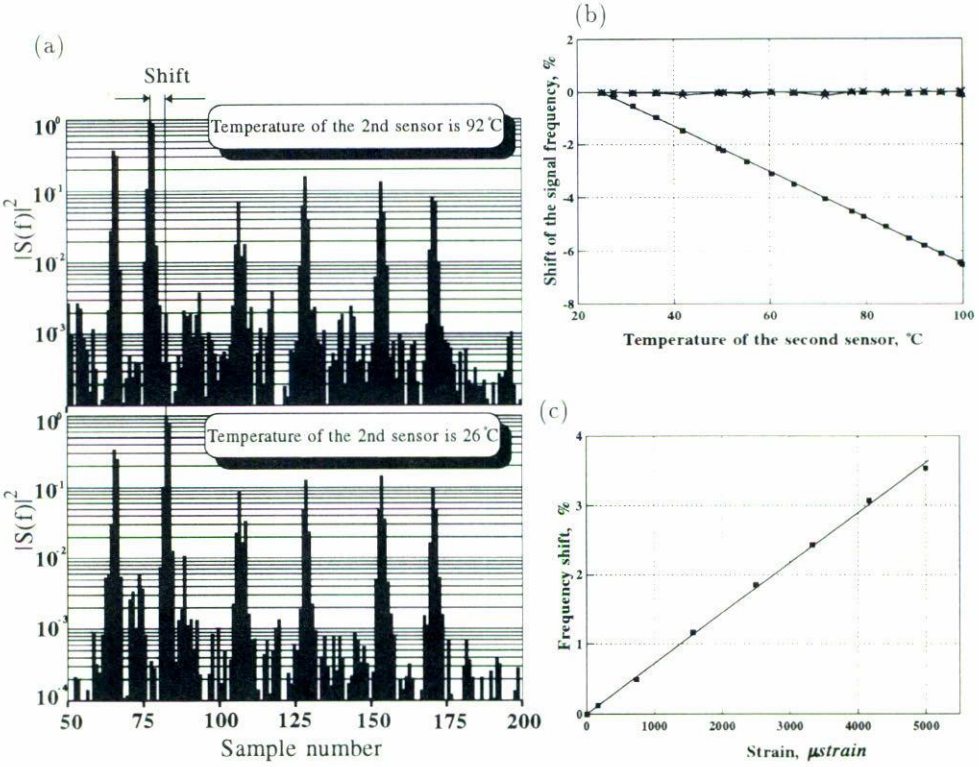

FIGURE 4. Quasi-distributed fiber-optic sensor: (a) Fourier transforms of output spectra at the temperature of the second local sensor 26°C and 92°C; (b) data on calibration of the second sensor (■ : experimental points, solid line: linear fitting), data for the first (×) and fifth (▲) local sensors are also shown (all local sensors except the second one were at an ambient temperature); and (c) dependence of frequency shift on axial strain at ambient temperature.

4. CONCLUSION

We have demonstrated a new technique for quasi-distributed temperature and strain sensing. Each local sensor is only formed by a pair of coupling points in a birefringent fiber. This is a relevant simplification in sensor fabrication. A compact grating spectrograph can be used to interrogate simultaneously a number of local sensors while maintaining high precision temperature or strain measurements. An approach to evaluate the influence of cross-talk, photodetector noise and fiber imperfections was presented. It may be useful for the optimization of a sensor in particular applications.

5. ACKNOWLEDGMENTS

Part of this work was performed while the stay of S.V. Miridonov and M.G. Shlyagin at the Centro de Investigación Científica y de Educación de Ensenada was supported by DAIC-Consejo Nacional de Ciencia y Tecnología.

REFERENCES

1. A.D. Kersey, *Proc. Soc. Photo-Opt. Instrum. Eng.* **2071** (1993) 30.
2. S.E. Kanellopoulos, V.A. Handerek, and A.J. Rojers, *Electron. Lett.* **30** (1994) 1786.
3. S.R. Taplin, A.Gh. Podoleanu, D.J. Webb, and D.A. Jackson, *Proc. Soc. Photo-Opt. Instrum. Eng.* **2292** (1994) 94.
4. S.A. Egorov, A.N. Mamaev, and A.S. Polyantsev, *J. Lightwave Technol.* **13** (1995) 1231.
5. V. Bhatia *et al., Meas. Sci. Technology* **7** (1996) 58.
6. M. Shlyagin, A. Khomenko, and D. Tentori, *Proc. Soc. Photo-Opt. Instrum. Eng.* **2730** (1996) 565.
7. A. Khomenko, M. Shlyagin, S. Miridonov, and D. Tentori, *Opt. Lett.* **18** (23) (1993) 2065.
8. M. Shlyagin, A. Khomenko, and D. Tentori, *Opt. Lett.* **20** (8) (1995) 869.